

CrossMark  
click for updatesCite this: *J. Mater. Chem. C*, 2015, 3,  
1309

# Fabrication of long-range ordered, broccoli-like SERS arrays and application in detecting endocrine disrupting chemicals†

Jing Chen,<sup>ab</sup> Gaowu Qin,<sup>\*a</sup> Wen Shen,<sup>b</sup> Yiyang Li<sup>c</sup> and Biswajit Das<sup>\*b</sup>

Periodic broccoli-shaped Au and Ag surface-enhanced Raman spectroscopy (SERS) arrays were fabricated by combining ordered SiO<sub>2</sub> colloidal crystal templates with the physical deposition technique. The SiO<sub>2</sub> colloidal crystal-assisted Au and Ag SERS substrates have a long-range, adjustable periodic structure and a clean surface without incorporating any reductants or surfactant chemicals. Different from depositing directly on the flat substrates, the colloidal crystal-assisted nanostructure array has a larger effective surface area under the same projected area of laser irradiation, which exposes more "hot spots". An increased roughness and a larger surface area have also been created as the highly bumpy surface feature of the broccoli-shaped SERS morphologies, resulting in a greater Raman amplification than the conventional metal film over nanosphere (MFON). SERS performances by Au and Ag SERS arrays reveal that the long-range broccoli-like morphology is a promising SERS platform as it is highly sensitive, reproducible and stable. The colloidal crystal-assisted Ag SERS array has a slightly higher enhancement factor (EF) than the Au SERS array, and they both are of the order of 10<sup>7</sup> enhancement. Compared to our previous work, which directly deposited noble metal nanoparticles onto flat substrates, the EF of the colloidal crystal-assisted SERS array is improved by one to two orders of magnitude. Finite-difference time-domain (FDTD) simulation was performed to estimate the electromagnetic field distribution. Finally, two endocrine disrupting chemicals (EDCs) (dioctyl phthalate (DOP) and dibutyl phthalate (DBP), homologous series) at different concentrations were successfully identified by Au and Ag SERS arrays with the detection limits of 0.24 × 10<sup>-9</sup> M and 0.22 × 10<sup>-9</sup> M, respectively. This study suggests that the broccoli-like Au and Ag SERS arrays are promising candidates for chemical sensing and this SERS substrate fabrication technique can be accessible to the standard industrial processes.

Received 4th October 2014  
Accepted 28th November 2014

DOI: 10.1039/c4tc02224f

[www.rsc.org/MaterialsC](http://www.rsc.org/MaterialsC)

## 1. Introduction

Endocrine disrupting chemicals (EDCs) encompass a variety of substances, both natural and man-made, including dioxin, alkylphenols, DDT, phthalates, polychlorinated biphenyls, and so forth, and can interfere with the hormone system in both humans and wildlife. EDCs may exist in many products people use daily such as plastic bottles, metal food cans, detergents, food, toys, cosmetics, and pesticides.<sup>1,2</sup> Exposure to EDCs can

increase the risk of developing reproductive cancers, cause lowered fertility, birth malformations, and sexual development problems.<sup>2,3</sup> In May 2011, a major phthalate-contaminated foodstuffs incident happened in Taiwan. Di(2-ethylhexyl) phthalate (DEHP) and diisononyl phthalate (DiNP) were illegally added to foods and beverages as a substitute for emulsifier.<sup>4,5</sup> Phthalates are one of EDCs that are closely related to human life because they are used as plasticizers in polyvinyl chloride (PVC) plastics.<sup>6</sup> As phthalates are not chemically bound to PVC, their molecules can evaporate to the atmosphere, or move into the foodstuff.<sup>7</sup> Phthalate exposure has been found to be associated with numerous reproductive health and developmental problems,<sup>6</sup> and phthalates exhibit low acute toxicity with LD<sub>50</sub> values of >1–30 g kg<sup>-1</sup> bodyweight.<sup>7</sup>

The increasing incidents about the general population being continuously and ubiquitously exposed to the EDCs have raised public concerns about the environmental contaminants and public health.<sup>8</sup> Hence, a robust, reliable assessment is strongly required to identify EDCs in the environmental media, foodstuff and consumer products.<sup>9,10</sup> The difficulties in detecting EDCs lie in the variety and the low concentrations. The

<sup>a</sup>Key Laboratory for Anisotropy and Texture of Materials (Ministry of Education), Northeastern University, Shenyang 110819, China. E-mail: qingw@smm.neu.edu.cn; Tel: +86 24 83691565

<sup>b</sup>Nevada Nanotechnology Center, Howard R. Hughes College of Engineering, University of Nevada, Las Vegas, NV 89154-4026, USA. E-mail: dasb@unlv.nevada.edu; Tel: +1 702 8952530

<sup>c</sup>Department of Electrical and Computer Engineering, University of Nevada, Las Vegas, NV 89154, USA

† Electronic supplementary information (ESI) available: FE-SEM images of SiO<sub>2</sub> colloidal crystal-assisted Ag SERS substrates at different deposition time (90 s, 180 s, and 300 s). EFs calculation of the broccoli-shaped Au and Ag SERS substrates. See DOI: 10.1039/c4tc02224f

traditionally used detection methods include high performance liquid chromatography,<sup>11</sup> high performance liquid chromatography-tandem mass spectrometry,<sup>5,8</sup> gas chromatography-mass spectrometry,<sup>12,13</sup> and gas chromatography-electron capture detector. These methods are highly robust; however, some features, such as requiring complex sample pretreatment, being time-consuming and having high cost, limit their applications.<sup>14</sup>

Surface-enhanced Raman spectroscopy (SERS) is a handy, low cost, fast, nondestructive, ultra-sensitive and information-rich analytical technique, which can fulfill trace detection or even single molecule detection.<sup>15–23</sup> Moreover, it provides fingerprint-like information, which can offer distinguishable vibrational information used for molecule identification, and the SERS peak intensity is related to the analyte concentration. All of these features make SERS applicable for identifying a wide variety of biological molecules,<sup>24–40</sup> including proteins, DNA, RNA, microorganisms, and cancer cells. They also make SERS an ideal approach for the detection of chemical molecules<sup>41–47</sup> such as toxic gases, explosives, drugs and EDCs. However, the detection of EDCs by the SERS methodology is an emerging research field, which needs more exploration. Moreover, several recently published papers in this realm were associated with the chemical preparation of SERS substrates,<sup>48,49</sup> which included surface chemistry and interfered with SERS measurements. Therefore, a new type of SERS substrate having the reliability, reproducibility, stability, and high-sensitivity is urgently needed.

To date, many methods have been developed for the preparation of SERS-active substrates,<sup>50–53</sup> and the modelling of SERS substrates can be summarized as mentioned below. (1) Metallic nanoparticles and metallic films.<sup>54–56</sup> Christou *et al.* reported that Au and Ag film SERS substrates were generated by using the single UV-laser pulse treatment of thin Au and Ag films supported on quartz glass.<sup>56</sup> Although this type of SERS substrate is among the most widely used due to their simple and cost-effective bottom-up fabrication approach, it is hard to predict the location of the “hot spots” in their random nanostructures, which results in low reproducibility. (2) Multi-branched metallic nanocrystals. In order to increase the surface roughness and surface area of spherical nanoparticles to create more “hot spots” and to allow more analyte molecules to be attached, the multi-branched metallic nanocrystals with spiky surface features have been developed.<sup>57–61</sup> Xie and co-workers reported flower-like Au nanocrystals that were chemically synthesized based on crystal growth in the limited ligand protection region.<sup>58</sup> Fang and co-workers demonstrated, using a nanoparticle-mediated aggregation protocol, that “sea urchin”-like gold mesoparticles can be synthesized *via* a secondary nucleation and growth process.<sup>60</sup> In the preparation of multi-branched metallic nanocrystals, surfactants are necessary for regulating the growth and stability of the nanocrystals. However, surfactants are hard to remove and retain on the nanocrystal surface, thus interfering with SERS detections. (3) Nanoparticle arrays. To reduce randomly aggregated colloids in SERS substrates, strategies like electrostatic assembly,<sup>62</sup> DNA hybridization-driven assembly,<sup>63</sup> or mechanical assembly, such as the convective flow upon solvent evaporation technique,<sup>64</sup>

have been investigated to tailor the spacing and obtain ordered nanoparticle arrays. In Wang's work, using cetyltrimethylammonium bromide (CTAB) as the capping surfactant, highly ordered, close-packed monolayer Au nanoparticle arrays with sub-10 nm gap were successfully formed.<sup>62</sup> Recently, Lim and co-workers described that by employing a DNA-modified technique, gold nanobridged nanogap particles with a uniform nanobridge-supported 1 nm interior gap were produced.<sup>63</sup> The abovementioned strategies are elaborate and can precisely control the interparticle distances and build well-defined SERS arrays. However, surface chemistry will still be involved as wet chemical routes are needed. Moreover, the operation procedures are relatively complicated. (4) Periodic SERS arrays. The periodic SERS array is one of the most prominent SERS substrates and has attracted great attention in recent years. Electron beam lithography (EBL) is famous for producing periodic SERS arrays. Yu *et al.* demonstrated that gold nanohole and nanodisk arrays with precisely controlled size and spacing could be fabricated by EBL.<sup>65</sup> Theiss and co-workers developed an electron beam lithography combined with an angle evaporation technique for the fabrication of Ag nanoparticle dimer arrays with separations of the order of 1 nm.<sup>66</sup> Despite the effectiveness of EBL, the time consuming, complex procedures, significant cost, low-throughput, and moderate enhancement factors (EF,  $\sim 10^5$ – $10^6$ ) hinder its wide applications. An alternative method for producing periodic SERS arrays is template-assisted fabrication, where porous anodic aluminium oxide (AAO),<sup>67</sup> natural nanostructures like butterfly wings,<sup>68</sup> polystyrene (PS),<sup>69</sup> or silica nanospheres<sup>70</sup> are popularly used as templates. Moreover, the template-assisted strategy allows for large-scale SERS arrays fabrication. In Rao's work, chemically reduced gold seeds were attached to the ordered functionalized silica colloidal spheres by electrostatic interaction, then the growth of gold nanoshells was applied as a SERS analytical tool to assess H<sub>2</sub>O<sub>2</sub> scavenging activity.<sup>70</sup> In the template-assisted approach, metal nanoparticles are often attached to the templates by covalent linkage or electrostatic interactions, thus involving surface chemistry and interfering with SERS measurements. Moreover, the SERS substrates made by the nanosphere lithography (NSL) technique often have a large interparticle distance, which is not suitable for SERS enhancement.

Despite the significant progress, obtaining reproducible, stable, reliable SERS substrates with novel geometries, periodic nanostructures, and high EFs over a large area in a convenient way still remains a challenge in SERS field. SERS nanostructures with features such as a delicate morphology and a highly rough surface are an attractive SERS candidate, and normally, a chemical approach is needed for fabricating this type of nanostructure as surfactants are necessary for regulating the transformation of shapes. However, surfactants will inevitably attach to the SERS substrate surface and interfere with SERS detections. For the physical deposition technique, it is difficult to get a delicate morphology directly, and normally, smooth metal films or unordered nanoparticle-aggregations will be fabricated.

In this paper, by skillfully combining a three-dimensional (3D) ordered SiO<sub>2</sub> colloidal crystal template and the physical deposition technique, delicate Au and Ag nanostructures with unique broccoli-like morphologies have been successfully fabricated under a series of appropriate parameters. Moreover, these broccoli-like Au and Ag nanostructures present long-range, periodic SERS arrays, and have clean, chemical-free surfaces. Therefore, their reliability and reproducibility have been guaranteed, and the highly bumpy surface feature ensures high-sensitivity. In general, the enhancement capability of the periodic patterned and highly reproducible SERS arrays is relatively low, whereas SERS substrates with a high enhancement capability are normally not reproducible.<sup>51</sup> Here, high reproducibility, periodic arrangement and large enhancement capability have been fulfilled at the same time in one SERS array. Therefore, the abovementioned limitations in the SERS substrates fabrication process have been well addressed.

The improvements and advantages of these novel SERS arrays are also reflected in the following aspects. (1) Compared to the conventional metal film over nanosphere (MFON) method,<sup>71</sup> more “hot spots” will be created and more analyte molecules will be attached to the broccoli-like SERS substrate, because the very bumpy SERS surface feature enables a greater surface roughness and a larger surface area. (2) Compared to the methods we developed previously by the deposition of metal nanoparticles onto the flat substrates directly,<sup>34,72</sup> the 3D long-range ordered SiO<sub>2</sub> colloidal crystal not only provides an arc surface to enable a larger surface area under the same projected area of the laser irradiation, but also makes an essential foundation for producing long-range periodic SERS arrays<sup>73</sup> and improves the reproducibility of SERS signals. Furthermore, by controlling the size of colloidal crystal spheres and the thickness of the metal nanoparticles deposited, the SERS substrates can be reproducibly produced.<sup>74</sup> (3) The physical fabrication technique was used for producing SERS substrates and no reductants or surfactant chemicals were involved, thus making it easy for the analyte molecules, particularly for the analytes with a weak affinity for the substrate surface, to access the “hot spots” regions by simple dripping or incubation of the substrate in the solution.<sup>53</sup> In addition, as the clean surfaces are without chemical interferences, the acquired SERS spectra are reliable. (4) This technique is convenient, cost-effective, allows high-throughput nanofabrication, and can be accessible to the standard industrial processes.

Next, the EFs, reproducibility, and long-term stability of these two SiO<sub>2</sub> colloidal crystal-assisted SERS arrays (Au and Ag) were evaluated. Finite-difference time-domain (FDTD) simulation was performed to estimate the electromagnetic field distribution. Then, these two SERS arrays were successfully applied to identify the two homologous series of EDCs, dioctyl phthalate (DOP) and dibutyl phthalate (DBP), and the detection limits were also calculated.

## 2. Experimental section

### 2.1 Chemicals and materials

DOP (99%), DBP (≥99.5%), rhodamine 6G (R6G) (≥95.0%, analytical standard), methanol (analytical standard) and ethanol (analytical standard) were purchased from Sigma-

Aldrich. Ammonium hydroxide (NH<sub>3</sub>·H<sub>2</sub>O, 50% v/v aq. soln.) and hydrogen peroxide (H<sub>2</sub>O<sub>2</sub>, 35% w/w aq. soln.) were purchased from Alfa Aesar. Tetraethyl orthosilicate (TEOS, 98%) and sulfuric acid (H<sub>2</sub>SO<sub>4</sub>, 95–98%) were purchased from GFS Chemicals. Gold targets (2.00" dia. × 0.125" thick, 99.99%) and silver targets (2.00" dia. × 0.25" thick, 99.99%) were purchased from Kurt J. Lesker Company (CA, USA). Silicon wafers were purchased from Silicon Valley Microelectronics (SVM, CA, USA). Ultrapure water (18.2 MΩ cm) was used throughout the experiment.

### 2.2 Synthesis of monodispersed SiO<sub>2</sub> spheres

Monodispersed SiO<sub>2</sub> spheres were produced using a slightly modified Stöber method.<sup>75</sup> Briefly, 4.5 mL of TEOS (98%) was rapidly added to a mixture of 9.0 mL of ammonium hydroxide solution (28%), 61.75 mL of ethanol, and 24.75 mL of H<sub>2</sub>O. The reaction mixture was kept under stirring for 2 h at room temperature. The produced monodispersed SiO<sub>2</sub> spheres were washed three times with water and ethanol by centrifugation at 7000g for 5 min, and then, the samples were kept in ethanol for the following procedures.

### 2.3 Fabrication of SiO<sub>2</sub> colloidal crystals

The vertical deposition method was employed. Briefly, a silicon wafer cleaned in fresh Piranha solution (concentrated H<sub>2</sub>SO<sub>4</sub>: 30% H<sub>2</sub>O<sub>2</sub> = 3 : 1 volume ratio. **Caution:** Piranha solution is extremely corrosive), was vertically attached to the inside wall of a plastic vessel containing SiO<sub>2</sub> colloidal suspension (SiO<sub>2</sub>-ethanol system, ~10 wt%). Then, using the isothermal heating evaporation method at 50 °C, SiO<sub>2</sub> colloidal crystals were self-assembled on the substrate surface. The entire system was kept in a stationary environment and isolated from external interference.

### 2.4 Preparation of Au and Ag SERS substrates

A versatile nanofabrication system (NanoSys 2, Oxford Applied Research Inc.), which can deposit nanoparticles of any material on any kind of substrate, was applied to deposit Au and Ag nanoparticles onto the abovementioned SiO<sub>2</sub> colloidal crystals template. This system basically consists of three parts: (1) the nanocluster source, (2) the quadrupole mass filter (QMF), and (3) the main deposition chamber. Nanoparticles with a large size distribution generated in the nanocluster source were filtered through the QMF, which was designed particularly for the high-resolution filtration of nanoparticles between 50 and 3 × 10<sup>6</sup> amu.<sup>76</sup> Here, for both Au and Ag nanoparticle deposition, the QMF was set at 10.0 nm size selection. The sputtering power was set at 115 W, which is a moderate value for the system, and this power can be adjusted to generate the appropriate sputtering rate after a series of testing. The flow rate of one of the aggregation gases, Ar, was 100 standard-state cubic centimeters per minute (scm), and the other aggregation gas, He, was 40 scm. The deposition rate (4.5 Å s<sup>-1</sup>) was measured using a quartz crystal monitor (QCM, Sigma Instruments, SQM-160).

## 2.5 SERS signal reproducibility and enhancement capability measurement

R6G was used as the probe molecule. 10  $\mu\text{L}$  of  $10^{-4}$  M R6G solution was dropped onto the abovementioned colloidal crystal-assisted Au and Ag SERS substrates. The SERS spectra were acquired immediately after the substrates were dried under ambient conditions. A normal Raman spectrum of  $10^{-2}$  M R6G solution was also acquired.

## 2.6 SERS detection of two kinds of EDCs

The methanol solutions of DOP and DBP at different concentrations ( $10^{-10}$ – $10^{-3}$  M) were prepared at first. For DOP detection, 200  $\mu\text{L}$  of DOP methanol solutions at different concentrations were dropped on the broccoli-like Au substrate. SERS signals were recorded after the methanol solvent completely evaporated. For DBP detection, the same procedures were performed but the broccoli-like Ag substrate was used.

## 2.7 Long-term stability measurement of the SERS substrates

The colloidal crystal-assisted Au and Ag SERS substrates were kept in commercial aluminum foil for 90 days, and then, their long-term stabilities were tested. R6G was employed as the probe molecule. The commercial aluminum foil was rinsed with acetone and ultrapure water in advance for degreasing.

## 2.8 Characterization

The morphologies of the  $\text{SiO}_2$  colloidal crystal and  $\text{SiO}_2$  colloidal crystal-assisted Au and Ag SERS substrates were observed by JEOL 7500F field emission scanning electron microscopy (FE-SEM). All SERS and bulk spectra were obtained using a confocal Horiba Jobin Yvon LabRAM HR Raman spectrometer equipped with a 785 nm laser and a  $100\times$  objective to focus the laser onto the sample surface and to collect the scattered light from samples. The incident laser power was attenuated to 0.8 mW for  $10^{-4}$  M of R6G SERS detection, and the laser power for the normal Raman spectra acquisition of  $10^{-2}$  M bulk R6G solution was set at 80 mW. The frequency of the Raman instrument was calibrated by referring to a silicon wafer at the vibrational band of  $520\text{ cm}^{-1}$ . All the measurements were carried out under ambient conditions.

# 3. Results and discussion

## 3.1 Fabrication of $\text{SiO}_2$ colloidal crystal

The initial diameter of the  $\text{SiO}_2$  spheres was approximately 230 nm. Fig. 1a reveals the surface features of the  $\text{SiO}_2$  colloidal crystal. We observed that a relatively uniform colloidal crystal film was assembled by  $\text{SiO}_2$  spheres self-arranged in a close-packed array, and the film also had a uniform thickness over large domains. However, the inevitable array defects still existed in certain microscopic areas in this  $\text{SiO}_2$  colloidal crystals array. One possible reason could be the non-uniformity of the  $\text{SiO}_2$  spheres size distribution, and the other possible reason might be the  $\text{SiO}_2$  spheres movement, caused by the electron-beam scanning during the SEM images collection.<sup>9</sup> Fig. 1b shows a

crevice in the  $\text{SiO}_2$  colloidal crystals, which reveals its 3D structure. The produced  $\text{SiO}_2$  colloidal crystal template paved the way for the next procedure in SERS substrate fabrication.

## 3.2 Fabrication of $\text{SiO}_2$ colloidal crystal-assisted Au and Ag SERS substrates, and SERS identification of two EDCs

Noble metal nanoparticles deposition on the substrates is a powerful technique for nanostructure fabrication. Instead of the deposition on the uncovered substrates directly, fabrication based on monolayer colloidal crystals or multilayer colloidal crystals is also an effective approach for producing a wide variety of nanostructures.<sup>77</sup> Different nanostructures with various morphologies can be produced by choosing proper deposition techniques and deposition conditions, and then the morphology-dependent properties and applications can be explored.<sup>77</sup>

Here, a  $\text{SiO}_2$  multilayer colloidal crystal template was used as the substrate, and Au and Ag nanoparticles were deposited onto the  $\text{SiO}_2$  spheres by employing a versatile nanocluster fabrication system (NanoSys 2, Oxford Applied Research Inc.). The QMF was turned on during the deposition process to control the nanoparticle size distribution, and a series of parameters were set to let the nanoparticles, sized around 10 nm, pass through and reach the  $\text{SiO}_2$  colloidal crystal template. The fabrication of  $\text{SiO}_2$  colloidal crystal-assisted Au and Ag SERS substrates, and the identification of EDCs are illustrated in Scheme 1.

Firstly, the deposition time was explored (ESI<sup>†</sup>), and 180 s was set as the optimal deposition time in this work. Fig. 1c and d are the corresponding FE-SEM images of the SERS substrates after deposition of Au and Ag nanoparticles, respectively, onto the  $\text{SiO}_2$  colloidal crystal templates (the deposition times were both 180 s). The insets in Fig. 1c and d show the corresponding high-magnification images. Interestingly, unique broccoli-shaped profiles were produced through this versatile nanofabrication system with proper deposition conditions, and large-area patterned broccoli-like Au and Ag SERS arrays were obtained. Compared to the conventional MFON substrates,<sup>71</sup> the highly rough surface feature and the enlarged surface area, together with large amounts of “hot spots” arise from the close interparticle distance on each “flower head”, enabling this broccoli-shaped SERS array to have a greater Raman amplification.

Next, the broccoli-shaped Au and Ag SERS substrates were applied to detect two EDCs, *i.e.* DOP and DBP, respectively. From Fig. 1e and f, the SERS spectra of DOP and DBP ( $10^{-6}$  M, methanol solutions) were obtained with a good ratio of signal to noise, and the sharp, distinguishable vibrational fingerprints they present, delivered the inherent structural information of the EDC molecules. DOP and DBP are homologous series (their structural formulas are displayed on the right side of Fig. 1e and f), and the acquired SERS spectra display different features. The major differences between these two SERS spectra are in the regions of  $780\text{--}920\text{ cm}^{-1}$  and  $1100\text{--}1150\text{ cm}^{-1}$ , which are assigned to the C–H out-of-plane bend and C–O stretch, respectively.<sup>78</sup> The fact that the colloidal crystal-assisted Au and Ag SERS substrates in this work have the ability to distinguish homologous series,

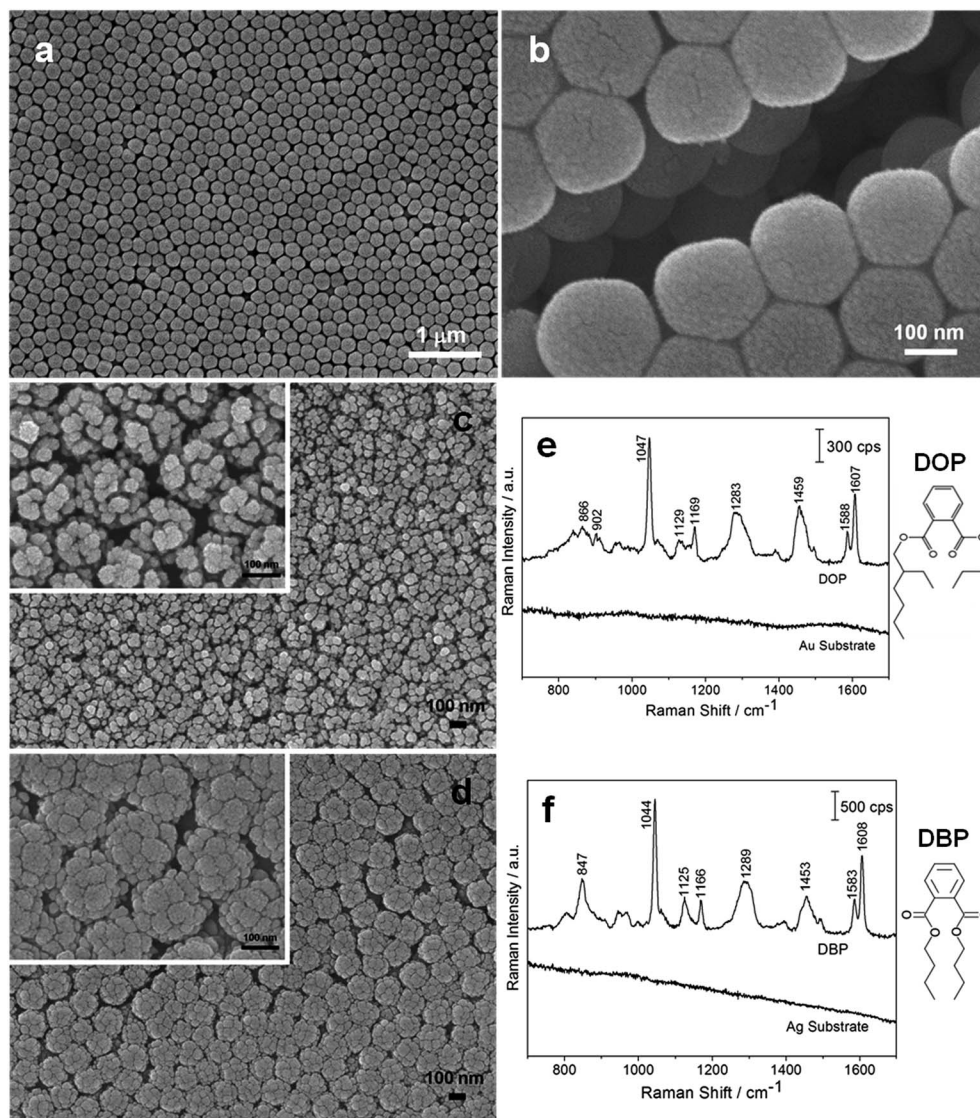


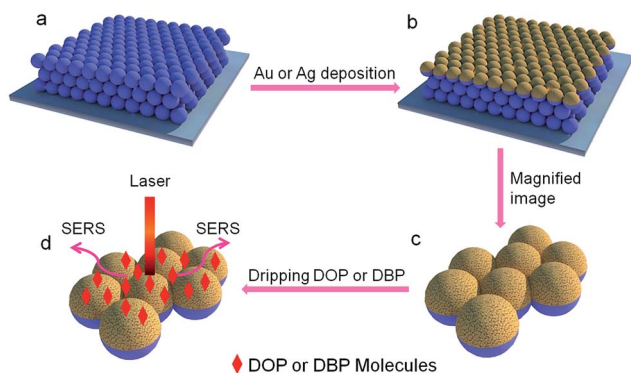
**Fig. 1** (a and b) FE-SEM images of SiO<sub>2</sub> colloidal crystals on a silicon wafer, and (b) reveals a crevice in the SiO<sub>2</sub> colloidal crystals. FE-SEM images of SERS substrates after deposition of (c) Au and (d) Ag nanoparticles onto the SiO<sub>2</sub> colloidal crystal templates, respectively (the deposition time were both 180 s), and the insets show the corresponding high-magnification images. (e) Top: SERS spectrum of 10<sup>-6</sup> M DOP methanol solution acquired from SiO<sub>2</sub> colloidal crystal-assisted Au SERS substrate; bottom: SERS spectrum obtained from the Au SERS substrate without dripping any EDCs. (f) Top: SERS spectrum of 10<sup>-6</sup> M DBP methanol solution acquired from SiO<sub>2</sub> colloidal crystal-assisted Ag SERS substrate; bottom: SERS spectrum obtained from the Ag SERS substrate without dripping any EDCs. Excitation wavelength: 785 nm; laser power: 8 mW. The collection time is 15 s exposure time and 5 scans. The structural formulas of DOP and DBP are displayed on the right sides of (e and f), respectively.

suggesting that the broccoli-shaped SERS arrays have a high sensitivity and the potential for wide applications in chemical molecules detection. Two flat SERS spectra at the bottom of Fig. 1e and f were acquired from the broccoli-shaped Au and Ag SERS substrates without dripping any EDCs. No evident Raman peaks could be detected, indicating clean surfaces without the incorporation of any reductants or surfactant chemicals, which is the fundamental principle for reliable SERS detection.

### 3.3 SERS reproducibility

Reproducibility is an important index for evaluating the performance of SERS substrates. Here, we chose R6G as the

probe molecule to explore the reproducibility of SiO<sub>2</sub> colloidal crystal-assisted Au and Ag SERS substrates. 10 μL of 10<sup>-4</sup> M R6G solution were dropped onto these two SERS substrates, and SERS spectra from 5 randomly selected spots on each SERS substrate were acquired under identical experimental conditions. The SERS spectra of R6G in these five different positions are fairly consistent with each other in terms of Raman peaks as well as Raman intensity (Fig. 2a and b). Fig. 2c gives even clearer clarification, from which the relative standard deviations (RSDs) of the peak intensity at 772 cm<sup>-1</sup> are about 8.7% and 5.7% for Fig. 2a and b, respectively. The low RSDs indicate good reproducibility and suggest the fabricated SiO<sub>2</sub> colloidal



**Scheme 1** Schematic diagrams of the fabrication of SiO<sub>2</sub> colloidal crystal-assisted Au and Ag SERS substrates and identification of EDCs. (a) SiO<sub>2</sub> colloidal crystals assembled on a silicon wafer; (b) after the deposition of Au or Ag nanoparticles on the SiO<sub>2</sub> colloidal crystal; (c) the corresponding high-magnification image; (d) SERS detection of DOP or DBP molecules by the SiO<sub>2</sub> colloidal crystal-assisted Au and Ag SERS substrates.

crystal-assisted Au and Ag SERS substrates in this work are reliable and good candidates for EDCs detection.

### 3.4 Electromagnetic simulation and EFs calculation

Numerical simulations were performed using the finite difference time domain (FDTD) method by employing a commercial software package from Lumerical Solutions, Inc., Canada (version 8.7.3), to numerically estimate the electromagnetic field distribution at the surface of the Au-coated and Ag-coated plasmonic nanostructures. The Yee cell in our calculation was set to 0.5 nm × 0.5 nm × 0.5 nm, and perfectly matched layers (PML) were used as a boundary condition. In order to match the experimental system as closely as possible, the models of the structures were developed by extracting from FE-SEM images. Subtle differences were found between the Au-coated (Fig. 3a) and Ag-coated (Fig. 3b) broccoli-shaped SERS arrays; therefore, typical regions (the area in each red circle in Fig. 3a and b) were selected separately for the FDTD simulations. Fig. 3c and d are the corresponding simulation models extracted from the typical

regions in Fig. 3a and b. Both Au and Ag nanoparticles were treated in spherical shapes and the diameter was 10 nm as the QMF was set at 10.0 nm size selection. The particles in a uniform dielectric medium ( $n = 1$ ) were illuminated from the top with a linearly polarized plane wave of 785 nm wavelength. The dielectric constants of Au and Ag were obtained from Johnson and Christy.<sup>79</sup> Fig. 3e and f show the corresponding simulation results of Au-coated and Ag-coated SERS array nanostructures. The electric field magnitude was normalized by dividing the maximum absolute value. The simulation results show that the broccoli-shaped SERS array structures generated localized plasmons, and substantial electromagnetic field enhancements were localized in the narrow gaps of the neighbouring nanoparticles (the nanoparticles constituted the “flower head” of the broccoli-like SERS array). These interparticle gaps are the “hot spots” that contribute largely to the SERS enhancement.

Next, the enhancement capability of the broccoli-shaped Au and Ag SERS substrates were evaluated by employing R6G as the probe molecules, and the EF of the broccoli-like Au substrate was calculated as  $1.12 \times 10^7$ , and the EF of the broccoli-like Ag substrate was calculated as  $1.45 \times 10^7$  (ESI† for details). Compared to our previous work,<sup>34,72</sup> which involved depositing Ag or Au nanoparticles onto the silicon wafer directly (the EF was  $10^5$  for the Ag substrate and  $10^6$  for the Au substrate in the previous work), the EF of the colloidal crystal-assisted Ag and Au SERS arrays in this work are testified to improve by  $10^2$  times and 10 times, respectively, which demonstrates the superiority of the broccoli-shaped nanostructure morphology.

### 3.5 Long-term stability of SERS substrates

In addition to Raman enhancement and reproducibility, stability is another important index for the SERS substrates, as an ideal SERS sensor system needs a long time and efficient running, which requires long-term stability without being degraded, contaminated, or loss of enhancement. Here, SiO<sub>2</sub> colloidal crystal-assisted Au and Ag SERS substrates were detected after they were saved in commercial aluminum foil for 90 days, and R6G was used as the probe molecule (Fig. 4). Each

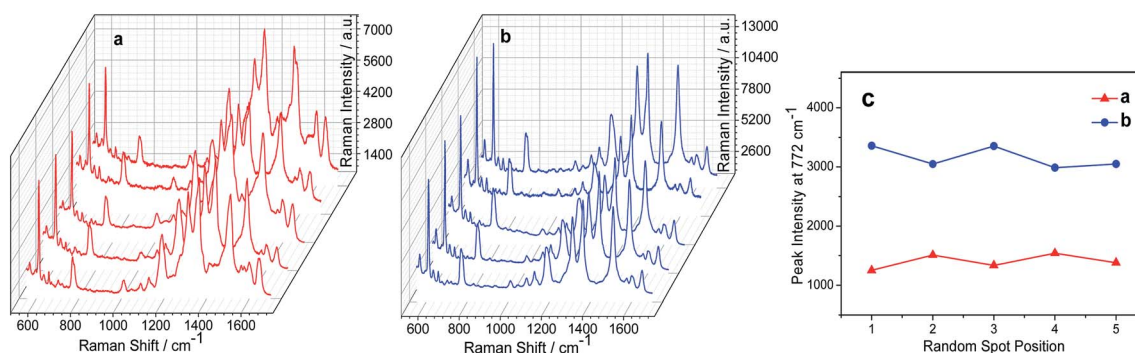


**Fig. 2** SERS spectra of  $10^{-4}$  M R6G acquired from 5 randomly selected places on the SiO<sub>2</sub> colloidal crystal-assisted (a) Au and (b) Ag SERS substrates (the deposition times were both 180 s). Excitation wavelength: 785 nm; laser power: 0.8 mW. The collection time was 15 s of exposure time and 5 scans. (c) Plots of the peak intensities of R6G at  $772 \text{ cm}^{-1}$  obtained from 5 random places on the abovementioned two SERS substrates.

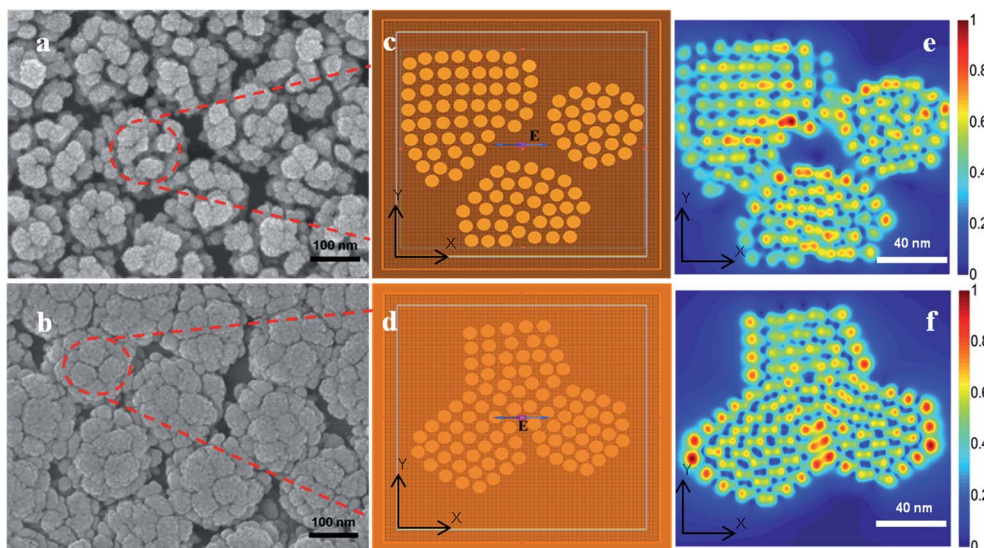


Fig. 3 FE-SEM images of (a) Au-coated and (b) Ag-coated broccoli-shaped SERS arrays (the deposition times were both 180 s). The regions in the red circles are the selected areas used for FDTD simulations. Simulation models for (c) Au-coated and (d) Ag-coated SERS arrays. The simulation results of (e) Au-coated and (f) Ag-coated broccoli-shaped SERS arrays.

SERS spectrum in Fig. 4a and b is an average result of five random detections focused on different positions. Compared to the colloid solution system, our SERS substrates display quite stable properties as they do not sediment out of solution. After 90 days, the SERS enhancement of the SiO<sub>2</sub> colloidal crystal-assisted Au substrate was reduced by 31.6%, and SiO<sub>2</sub> colloidal crystal-assisted Ag substrate was reduced by 51.2% (average results of the vibration mode at 772 cm<sup>-1</sup>, 1188 cm<sup>-1</sup>, and 1508 cm<sup>-1</sup>) relative to the SERS spectra in Fig. S2b and S2c (ESI<sup>†</sup>), respectively, which were obtained from the freshly prepared SERS substrates. The long-term stability data of the broccoli-shaped Au and Ag SERS substrates in this work are comparable to that of Halas's work<sup>62</sup> and Kim's work.<sup>80</sup> We can conclude that in this work, the colloidal crystal-assisted Ag SERS

array has a slightly higher EF than the Au SERS array, whereas the latter has a better long-term stability than the Ag SERS array, which may result from Ag nanoparticles being easily oxidized under ambient conditions.

### 3.6 Relationship between SERS intensity and two EDCs concentration

A series of SERS spectra of DOP (Fig. 5a) and DBP (Fig. 5b) at different concentrations (10<sup>-10</sup> to 10<sup>-3</sup> M, methanol solutions) were obtained to demonstrate the sensitivity of the broccoli-shaped SERS substrates. From Fig. 5a and b, the SERS spectral intensity decreases as the concentration decreases. The detection limits of 0.24 × 10<sup>-9</sup> M and 0.22 × 10<sup>-9</sup> M were obtained for the broccoli-shaped Au and Ag SERS arrays for detecting DOP and DBP respectively (according to the signal/noise ratio of three). The correlations between SERS intensity and DOP, DBP concentration are listed in Fig. 5c and d, respectively. The SERS peak intensities of DOP at 1047 cm<sup>-1</sup> and DBP at 1044 cm<sup>-1</sup> were set as the y-axis, and DOP and DBP concentration (logarithmic) was set as the x-axis.

Two linear relationships exist in the concentration range of 10<sup>-10</sup>–10<sup>-3</sup> M for both DOP and DBP. For DOP, when in the concentration range of 10<sup>-10</sup>–10<sup>-6</sup> M, the linear regression equation is  $y = 327.2 \log(x) + 3229.8$ , and the correlation coefficient is 0.991 ( $n = 5$ ); when in the concentration range of 10<sup>-6</sup>–10<sup>-3</sup> M, the linear regression equation is  $y = 1506.9 \log(x) + 10\,238.3$ , and the correlation coefficient is 0.996 ( $n = 4$ ). For DBP, when in the concentration range of 10<sup>-10</sup>–10<sup>-5</sup> M, the linear regression equation is  $y = 722.1 \log(x) + 7007.1$ , and the correlation coefficient is 0.990 ( $n = 6$ ); when in the concentration range of 10<sup>-5</sup>–10<sup>-3</sup> M, the linear regression equation is  $y = 2900 \log(x) + 18\,160$ , and the correlation coefficient is 0.999 ( $n = 3$ ).

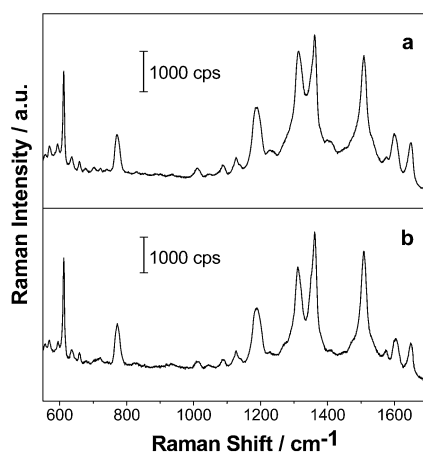


Fig. 4 SERS spectrum of 10<sup>-4</sup> M R6G solution acquired from SiO<sub>2</sub> colloidal crystal-assisted (a) Au and (b) Ag SERS substrates after they were kept in commercial aluminum foil under ambient conditions for 90 days. Laser power: 0.8 mW.

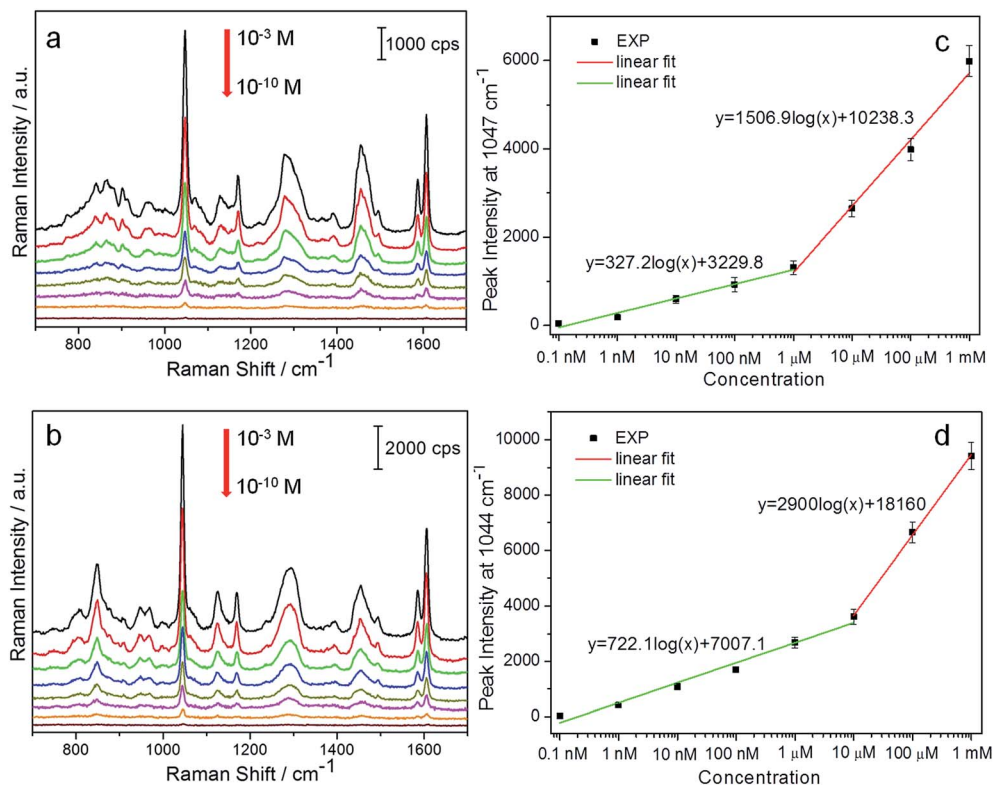


Fig. 5 Concentration-dependent SERS spectra of (a) DOP ( $10^{-10}$ – $10^{-3}$  M, methanol solutions), which were obtained from the broccoli-shaped Au SERS substrate, and (b) DBP ( $10^{-10}$ – $10^{-3}$  M, methanol solutions), which were obtained from the broccoli-shaped Ag SERS substrate. Excitation wavelength: 785 nm; laser power: 8 mW. Piecewise linear plots of (c) DOP SERS intensity at  $1047\text{ cm}^{-1}$  vs. DOP concentration in (a), and (d) DBP SERS intensity at  $1044\text{ cm}^{-1}$  vs. DBP concentration in (b).

According to the two different linear relationships in the entire concentration range, we conjecture that there may exist submonolayer-monolayer adsorption (in the low-concentration range) and multilayer adsorption (in the high-concentration range), following two different types of adsorption isotherms.<sup>81,82</sup> In the low-concentration region, because all the analyte molecules are in contact with the SERS substrate surface directly and SERS has proximity effect, SERS intensity increases sharply as the analyte concentration increases. However, in the high-concentration region, because of the multilayer adsorption, SERS intensity increase becomes slower. We should note that, in Fig. 5c and d, the  $x$ -axis has taken the logarithm values; therefore, the slopes in the low-concentration region are smaller than that in the high-concentration region. In Cheng's work,<sup>82</sup> this piecewise linear phenomenon has also been reported, and they also mentioned the fact that the slope in the high-concentration linear range ( $x$ -axis did not take the logarithm values) and reflected the multilayer adsorption responsible for the weak enhancement.<sup>82</sup> In Fig. 5c and d, the inflection point of the piecewise linearity of DOP comes at a lower concentration ( $10^{-6}$  M) in comparison to DBP's ( $10^{-5}$  M), and this may result from DOP having a larger molecular 3D structure than DBP; thus, monolayer adsorption saturation comes at a lower concentration than that of DBP.

## 4. Conclusions

Au and Ag nanoparticles were deposited onto  $\text{SiO}_2$  multilayer colloidal crystal templates by a versatile nanocluster fabrication system and broccoli-shaped Au and Ag SERS substrates were produced. This SERS array has a long-range, controllable periodic structure, and also has a clean surface without incorporating any reductants or surfactant chemicals. The broccoli-shaped SERS morphology creates an increased roughness and a larger surface area, resulting in a greater Raman amplification than the conventional MFON. SERS performances by these two SERS arrays reveal that this long-range broccoli-like morphology is a promising SERS platform as it is highly sensitive, reproducible, and has long-term stability. The EFs of the two broccoli-like Au and Ag SERS arrays are both high, up to  $10^7$ . Compared to our previous work, which involved depositing noble metal nanoparticles onto the flat substrates directly, the EF of the colloidal crystal-assisted SERS array is improved by one to two orders of magnitude. The FDTD simulation results show that substantial electromagnetic field enhancement exists in the gaps between nanoparticles on the "flower head". Finally, two EDCs (*i.e.* DOP and DBP, methanol solutions) at different concentrations were successfully identified by the broccoli-like Au and Ag SERS substrates with the detection limits of  $0.24 \times 10^{-9}$  M and  $0.22 \times 10^{-9}$  M, respectively. It is hopeful that this colloidal crystals-assisted nanostructure arrays with the

unique broccoli-shaped profile will become a promising candidate in SERS sensing.

## Acknowledgements

We thank UNLV Genomics Core Facility for assistance with ultrapure water. We thank Dr Frank van Breukelen and Dr Peipei Pan from UNLV for assistance with the centrifuge. This work was supported by the National Natural Science Foundation of China (no. 50871028), Changjiang Scholars and Innovative Research Team in University (no. IRT0713), and the Fundamental Research Funds for the Central Universities (no. N110610001 and N110810001). J. Chen appreciates the assistance from China Scholarship Council (CSC), and Northeastern University excellent doctoral dissertation breeding program, China.

## References

- 1 <http://www.niehs.nih.gov/health/topics/agents/endocrine/>.
- 2 [http://en.wikipedia.org/wiki/Endocrine\\_disruptor](http://en.wikipedia.org/wiki/Endocrine_disruptor).
- 3 R. M. Harrison and R. E. Hester, *Endocrine Disrupting Chemicals*, Royal Society of Chemistry, Cambridge, UK, 1999.
- 4 J. Yang, R. Hauser and R. H. Goldman, *Food Chem. Toxicol.*, 2013, **58**, 362–368.
- 5 M. T. Wu, C. F. Wu, J. R. Wu, B. H. Chen, E. K. Chen, M. C. Chao, C. K. Liu and C. K. Ho, *Environ. Int.*, 2012, **44**, 75–79.
- 6 V. R. Preedy, *Handbook of Growth and Growth Monitoring in Health and Disease*, Springer, 2012, vol. 1.
- 7 U. Heudorf, V. Mersch-Sundermann and J. Angerer, *Int. J. Hyg. Environ. Health*, 2007, **210**, 623–634.
- 8 H. M. Koch, A. Haller, T. Weiss, H. U. Kafferlein, J. Stork and T. Bruning, *Toxicol. Lett.*, 2012, **213**, 100–106.
- 9 C. Fang, N. M. Bandaru, A. V. Ellis and N. H. Voelcker, *Biosens. Bioelectron.*, 2013, **42**, 632–639.
- 10 T. H. Yen, D. T. Lin-Tan and J. L. Lin, *J. Formosan Med. Assoc.*, 2011, **110**, 671–684.
- 11 G. Tranfo, L. Caporossi, E. Paci, C. Aragona, D. Romanzi, C. De Carolis, M. De Rosa, S. Capanna, B. Papaleo and A. Pera, *Toxicol. Lett.*, 2012, **213**, 15–20.
- 12 J. Sanchez-Avila, R. Tauler and S. Lacorte, *Environ. Int.*, 2012, **46**, 50–62.
- 13 T. Fierens, M. Van Holderbeke, H. Willems, S. De Henauw and I. Sioen, *Food Chem. Toxicol.*, 2012, **50**, 2945–2953.
- 14 W. Cheung, I. T. Shadi, Y. Xu and R. Goodacre, *J. Phys. Chem. C*, 2010, **114**, 7285–7290.
- 15 S. M. Nie and S. R. Emory, *Science*, 1997, **275**, 1102–1106.
- 16 K. Kneipp, Y. Wang, H. Kneipp, L. T. Perelman, I. Itzkan, R. Dasari and M. S. Feld, *Phys. Rev. Lett.*, 1997, **78**, 1667–1670.
- 17 R. Zhang, Y. Zhang, Z. C. Dong, S. Jiang, C. Zhang, L. G. Chen, L. Zhang, Y. Liao, J. Aizpurua, Y. Luo, J. L. Yang and J. G. Hou, *Nature*, 2013, **498**, 82–86.
- 18 S. L. Kleinman, E. Ringe, N. Valley, K. L. Wustholz, E. Phillips, K. A. Scheidt, G. C. Schatz and R. P. Van Duyne, *J. Am. Chem. Soc.*, 2011, **133**, 4115–4122.
- 19 A. M. Michaels, M. Nirmal and L. E. Brus, *J. Am. Chem. Soc.*, 1999, **121**, 9932–9939.
- 20 P. J. Moyer, J. Schmidt, L. M. Eng and A. J. Meixner, *J. Am. Chem. Soc.*, 2000, **122**, 5409–5410.
- 21 X. M. Qian and S. M. Nie, *Chem. Soc. Rev.*, 2008, **37**, 912–920.
- 22 D. K. Lim, K. S. Jeon, H. M. Kim, J. M. Nam and Y. D. Suh, *Nat. Mater.*, 2010, **9**, 60–67.
- 23 J. P. Camden, J. A. Dieringer, J. Zhao and R. P. Van Duyne, *Acc. Chem. Res.*, 2008, **41**, 1653–1661.
- 24 X. M. Qian, X. H. Peng, D. O. Ansari, Q. Yin-Goen, G. Z. Chen, D. M. Shin, L. Yang, A. N. Young, M. D. Wang and S. M. Nie, *Nat. Biotechnol.*, 2008, **26**, 83–90.
- 25 J. D. Driskell, A. G. Seto, L. P. Jones, S. Jokela, R. A. Dluhy, Y. P. Zhao and R. A. Tripp, *Biosens. Bioelectron.*, 2008, **24**, 917–922.
- 26 E. A. Pozzi, M. D. Sonntag, N. Jiang, J. M. Klingsporn, M. Hersam and R. P. Van Duyne, *ACS Nano*, 2013, **7**, 885–888.
- 27 G. F. Wang, R. J. Lipert, M. Jain, S. Kaur, S. Chakraborty, M. P. Torres, S. K. Batra, R. E. Brand and M. D. Porter, *Anal. Chem.*, 2011, **83**, 2554–2561.
- 28 M. Lee, S. Lee, J. H. Lee, H. W. Lim, G. H. Seong, E. K. Lee, S. I. Chang, C. H. Oh and J. Choo, *Biosens. Bioelectron.*, 2011, **26**, 2135–2141.
- 29 M. Y. Sha, H. Xu, S. G. Penn and R. Cromer, *Nanomedicine*, 2007, **2**, 725–734.
- 30 S. Shanmukh, L. Jones, J. Driskell, Y. P. Zhao, R. Dluhy and R. A. Tripp, *Nano Lett.*, 2006, **6**, 2630–2636.
- 31 P. Negri, A. Kage, A. Nitsche, D. Naumann and R. A. Dluhy, *Chem. Commun.*, 2011, **47**, 8635–8637.
- 32 J. A. Dougan, D. MacRae, D. Graham and K. Faulds, *Chem. Commun.*, 2011, **47**, 4649–4651.
- 33 Z. A. Combs, S. Chang, T. Clark, S. Singamaneni, K. D. Anderson and V. V. Tsukruk, *Langmuir*, 2011, **27**, 3198–3205.
- 34 J. Chen, G. W. Qin, J. S. Wang, J. Y. Yu, B. Shen, S. Li, Y. P. Ren, L. Zuo, W. Shen and B. Das, *Biosens. Bioelectron.*, 2013, **44**, 191–197.
- 35 J. Chen, B. Shen, G. W. Qin, X. W. Hu, L. H. Qian, Z. W. Wang, S. Li, Y. P. Ren and L. Zuo, *J. Phys. Chem. C*, 2012, **116**, 3320–3328.
- 36 T. Smith-Palmer, C. Douglas and P. Fredericks, *Vib. Spectrosc.*, 2010, **53**, 103–106.
- 37 X. Y. Zhang, M. A. Young, O. Lyandres and R. P. Van Duyne, *J. Am. Chem. Soc.*, 2005, **127**, 4484–4489.
- 38 X. X. Han, B. Zhao and Y. Ozaki, *Anal. Bioanal. Chem.*, 2009, **394**, 1719–1727.
- 39 A. Barhoumi and N. J. Halas, *J. Am. Chem. Soc.*, 2010, **132**, 12792–12793.
- 40 G. S. Hong, C. Li and L. M. Qi, *Adv. Funct. Mater.*, 2010, **20**, 3774–3783.
- 41 D. L. Stokes, A. Pal, V. A. Narayanan and T. Vo-Dinh, *Anal. Chim. Acta*, 1999, **15**, 265–274.
- 42 D. A. Stuart, K. B. Biggs and R. P. Van Duyne, *Analyst*, 2005, **131**, 568–572.
- 43 B. D. Piorek, S. J. Lee, J. G. Santiago, M. Moskovits, S. Banerjee and C. D. Meinhart, *Proc. Natl. Acad. Sci. U. S. A.*, 2007, **104**, 18898–18901.

- 44 M. Lin, L. He, J. Awika, L. Yang, D. R. Ledoux, H. Li and A. Mustapha, *J. Food Sci.*, 2008, **73**, 129–134.
- 45 R. S. Golightly, W. E. Doering and M. J. Natan, *ACS Nano*, 2009, **3**, 2859–2869.
- 46 R. A. Halvorson and P. J. Vikesland, *Environ. Sci. Technol.*, 2010, **44**, 7749–7755.
- 47 K. V. Kong, Z. Y. Lam, W. K. O. Lau, W. K. Leong and M. Oivo, *J. Am. Chem. Soc.*, 2013, **135**, 18028–18031.
- 48 Q. An, P. Zhang, J. M. Li, W. F. Ma, J. Guo, J. Hu and C. C. Wang, *Nanoscale*, 2012, **4**, 5210–5216.
- 49 X. Z. Li, S. Zhang, Z. Yu and T. Y. Yang, *Appl. Spectrosc.*, 2014, **68**, 483–487.
- 50 S. C. Luo, K. Sivashanmugan, J. D. Liao, C. K. Yao and H. C. Peng, *Biosens. Bioelectron.*, 2014, **61**, 232–240.
- 51 D. Cialla, A. Marz, R. Bohme, F. Theil, K. Weber, M. Schmitt and J. Popp, *Anal. Bioanal. Chem.*, 2012, **403**, 27–54.
- 52 Y. Q. Wang, B. Yan and L. X. Chen, *Chem. Rev.*, 2013, **113**, 1391–1428.
- 53 S. L. Kleinman, R. R. Frontiera, A. I. Henry, J. A. Dieringer and R. P. Van Duyne, *Phys. Chem. Chem. Phys.*, 2013, **15**, 21–36.
- 54 J. B. Jackson and N. J. Halas, *Proc. Natl. Acad. Sci. U. S. A.*, 2004, **101**, 17930–17935.
- 55 R. Prucek, A. Panacek, J. Soukupova, R. Novotny and L. Kvitek, *J. Mater. Chem.*, 2011, **21**, 6416–6420.
- 56 K. Christou, I. Knorr, J. Ihlemann, H. Wackerbarth and V. Beushausen, *Langmuir*, 2010, **26**, 18564–18569.
- 57 M. Schutz, D. Steinigeweg, M. Salehi, K. Kompe and S. Schlucker, *Chem. Commun.*, 2011, **47**, 4216–4218.
- 58 J. P. Xie, Q. B. Zhang, J. Y. Lee and D. I. C. Wang, *ACS Nano*, 2008, **2**, 2473–2480.
- 59 J. J. Fu, W. C. Ye and C. M. Wang, *Mater. Chem. Phys.*, 2013, **141**, 107–113.
- 60 J. X. Fang, S. Y. Du, S. Lebedkin, Z. Y. Li, R. Kruk, M. Kappes and H. Hahn, *Nano Lett.*, 2010, **10**, 5006–5013.
- 61 M. Yang, R. Alvarez-Puebla, H. S. Kim, P. Aldeanueva-Potel, L. M. Liz-Marzan and N. A. Kotov, *Nano Lett.*, 2010, **10**, 4013–4019.
- 62 H. Wang, C. S. Levin and N. J. Halas, *J. Am. Chem. Soc.*, 2005, **127**, 14992–14993.
- 63 D. K. Lim, K. S. Jeon, J. H. Hwang, H. Kim, S. Kwon, Y. D. Suh and J. M. Nam, *Nat. Nanotechnol.*, 2011, **6**, 452–460.
- 64 K. D. Alexander, M. J. Hampton, S. P. Zhang, A. Dhawan, H. X. Xu and R. Lopez, *J. Raman Spectrosc.*, 2009, **40**, 2171–2175.
- 65 Q. M. Yu, P. Guan, D. Qin, G. Golden and P. M. Wallace, *Nano Lett.*, 2008, **8**, 1923–1928.
- 66 J. Theiss, P. Pavaskar, P. M. Echternach, R. E. Muller and S. B. Cronin, *Nano Lett.*, 2010, **10**, 2749–2754.
- 67 Z. X. Luo, A. D. Peng, H. B. Fu, Y. Ma, J. N. Yao and B. H. Loo, *J. Mater. Chem.*, 2008, **18**, 133–138.
- 68 N. L. Garrett, P. Vukusic, F. Ogrin, E. Sirotkin, C. P. Winlove and J. Moger, *J. Biophotonics*, 2009, **2**, 157–166.
- 69 J. M. Li, W. F. Ma, C. Wei, J. Guo, J. Hu and C. C. Wang, *J. Mater. Chem.*, 2011, **21**, 5992–5998.
- 70 Y. Y. Rao, Q. F. Chen, J. Dong and W. P. Qian, *Analyst*, 2011, **136**, 769–774.
- 71 L. A. Dick, A. D. McFarland, C. L. Haynes and R. P. Van Duyne, *J. Phys. Chem. B*, 2002, **106**, 853–860.
- 72 J. Chen, W. Shen, D. Biswajit, Y. Y. Li and G. W. Qin, *RSC Adv.*, 2014, **4**, 22660–22668.
- 73 L. Lu and A. Eychmuller, *Acc. Chem. Res.*, 2008, **41**, 244–253.
- 74 M. Culha, B. Cullum, N. Lavrik and C. K. Klutse, *J. Nanotechnol.*, 2012, 971380.
- 75 T. R. Zhang, Q. Zhang, J. P. Ge, J. Goebel, M. W. Sun, Y. S. Yan, Y. S. Liu, C. L. Chang, J. H. Guo and Y. D. Yin, *J. Phys. Chem. C*, 2009, **113**, 3168–3175.
- 76 A. Banerjee and B. Das, *Rev. Sci. Instrum.*, 2008, **79**, 033910.
- 77 X. Z. Ye and L. M. Qi, *Nano Today*, 2011, **6**, 608–631.
- 78 K. A. Rubinson and J. F. Rubinson, *Contemporary Instrumental Analysis*, Prentice Hall, USA, 1999.
- 79 P. B. Johnson and R. W. Christy, *Phys. Rev. B: Solid State*, 1972, **6**, 4370–4379.
- 80 S. Choi, M. Ahn and J. Kim, *Anal. Chim. Acta*, 2013, **779**, 1–7.
- 81 S. Brunauer, L. S. Deming, W. E. Deming and E. Teller, *J. Am. Chem. Soc.*, 1940, **62**, 1723–1732.
- 82 H. W. Cheng, S. Y. Huan, H. L. Wu, G. L. Shen and R. Q. Yu, *Anal. Chem.*, 2009, **81**, 9902–9912.